Title:

Optimal cell length for exploration and exploitation in chemotactic planktonic bacteria

Keywords: bacterial shape, chemotaxis, cell length, *Escherichia coli*, Individual-Based Models, microbial individual based ecology, phycosphere.

Authors: Òscar Guadayol[1*], Rudi Schuech[2], Stuart Humphries[3]

Affiliations:

[1] Mediterranean Institute for Advanced Studies, IMEDEA (UIB-CSIC), Miquel Marqués 21, 07190 Esporles, Balearic Islands, Spain

[2] Department of Mathematics and Center for Computational Science, Tulane University, New Orleans, LA 70118, USA

[3] School of Life Sciences, Joseph Banks Laboratories, University of Lincoln, Lincoln LN6 7DL, UK

* Correspondence to: oscar@guadayol.cat

Competing Interests: No competing interests are declared.

Abstract

Elongated morphologies are prevalent among marine motile bacterioplankton. This is often attributed to enhanced chemotactic ability, but how long is best? We hypothesized the existence of an optimal cell length for efficient chemotaxis resulting from shape-imposed physical constraints acting on the trade-off between rapid exploration versus efficient exploitation of nutrient sources. To test this hypothesis, we first evaluated the chemotactic performance of elongated cephalexin-treated *Escherichia coli* towards α-methyl-aspartate in an agarose-based microfluidic device that creates linear, stable and quiescent chemical gradients. Our experiments showed that cells of

intermediate lengths aggregated most tightly to the chemoattractant source. We then replicated these experimental results with Individual Based Model (IBM) simulations. A sensitivity analysis of the IBM allowed us to gain mechanistic insights into which parameters drive this trend and showed that the poor chemotactic performance of very short cells is caused by loss of directionality, whereas long cells are penalized by brief, slow runs. Finally, we evaluated the chemotactic performance of cells of different length with IBM simulations of a phycosphere – a hotspot of microbial interactions in the ocean. Results indicated that long cells swimming in a run-and-reverse pattern with extended runs and moderate speeds are most efficient at harvesting nutrients in this microenvironment. The combination of microfluidic experiments and IBMs proves thus to be a powerful tool for untangling the physical constraints that motile bacteria are facing in the ocean.

Introduction

Shape is a functional trait that influences several important tasks in bacterial life, including motility, nutrient uptake, resistance to grazing, passive dispersion, and pathogenicity (Young, 2006). Among the characters commonly used to parametrize microbial shape, cell length exhibits one of the highest degrees of variability. Not only is there considerable interspecific diversity in cell length but also intraspecific. Cell length may fluctuate throughout the cell cycle and depends on growth rate and nutritional environment (Vadia & Levin, 2015; Willis & Huang, 2017), and sometimes increases dramatically as stressed individuals stop dividing (Erill et al, 2007).

One of the most important behaviours that planktonic bacteria can undertake is chemotaxis, which allows a motile bacterium to detect and track chemical gradients (exploration) and remain close to a nutrient source to maximize uptake (exploitation). Elongated cell morphologies are particularly prevalent among planktonic chemotactic bacteria (Dusenbery, 1998) probably because they help microbial swimmers overcome the most insidious challenge they face: Brownian motion. Swimming bacteria live in a low Reynolds number regime and, due to their small size, cannot maintain a straight course as they are constantly deflected by colliding water molecules. To overcome this challenge, flagellated bacteria have evolved a characteristic swimming pattern,

consisting of a sequence of runs and sudden reorientations. During a run, a cell swims in a relatively straight line, while in the reorientation phase the direction of motion changes in species-specific ways (Mitchell, 2002; Mitchell & Kogure, 2006; Grognot & Taute, 2021). Elongation, by increasing rotational drag, reduces the effects of Brownian motion, thus allowing longer and straighter runs and increasing signal-to-noise ratios and chemotactic performance (Dusenbery, 2009). Furthermore, the increase in rotational drag due to elongation also restricts reorientation angles (Guadayol et al, 2017), which helps cells to track gradients more rapidly (Locsei, 2007; Nicolau et al, 2009).

However, elongation also poses some challenges to efficient chemotaxis. First, the restriction of reorientation angles leads to higher dispersal rates (Lovely & Dahlquist, 1975) and so shortens the time spent close to a nutrient source. Second, elongation increases translational friction, slowing the cell and decreasing swimming efficiency (Dusenbery, 1998; Schuech et al, 2019). And finally, it can slow down or weaken the cell's response to environmental cues as, given the diffusive nature of intracellular transport of signals, the time it takes for chemotactic signals to travel from the membrane receptors to the flagellar motors increases quadratically with cell length (Segall et al, 1985). In bacteria with randomly distributed multiple flagella, this signal delay can also induce desynchronization of flagella (Maki et al, 2000), ultimately leading to alterations in the motility pattern (Guadayol et al, 2017).

Thus, current theories predict both potential advantages and disadvantages of elongation for chemotaxis (see section *Theoretical Background* and Table S1 in supplementary materials). We hypothesized that optimal cell lengths for efficient chemotaxis exist, imposed by a trade-off between the need to run straight, swim efficiently, and explore the environment quickly, and the need to reorient when desired, respond promptly to environmental changes, and maximize the time spent near nutrient sources.

We sought to experimentally test our hypothesis by using *Escherichia coli* cultures treated with cephalexin, an antibiotic that stops cells from dividing without otherwise physiologically

impairing them (Rolinson, 1980; Ishihara et al, 1983; Maki et al, 2000). To assess the influence of cell length on chemotactic performance, we subjected cultures at various stages of elongation to microfluidic chemotactic assays with different gradients of concentration of the chemoattractant α-methyl-aspartate. Our experimental results support the hypothesis that optimal chemotaxis occurs at intermediate cell lengths. To gain a mechanistic understanding of the observed trend, we then built an individual based model (IBM) of our experimental system in which the chemotactic behaviour was simulated with a well-known model for the aspartate chemotactic pathway in *E. coli* (Tu et al, 2008). We used this IBM to further explore the consequences of elongation for chemotaxis in the phycosphere, the chemically distinct area surrounding phytoplanktonic cells where most interactions with bacteria, with global significance, take place (Seymour et al, 2017; Raina et al, 2022).

Methods

Cultures

Experiments were performed with the chemotactic *Escherichia coli* strain AW405. Cultures were grown overnight at 30ºC in 25 mL of minimum growth media (Maki et al, 2000) from frozen glycerol stock and shaken at 200 rpm at an orbit of 19 mm in 100mL Erlenmeyer flasks. The saturated culture was diluted 100-fold in 25 mL of fresh medium. Growth was monitored hourly using a cell density meter measuring at a wavelength of 600nm. After ~2h, once cultures had achieved exponential growth (optical density ~0.2), a sample was taken to conduct a chemotactic assay on the non-treated population, and then cephalexin was added to a final concentration of 60μgL^{-1}. Cephalexin is a β-lactam antibiotic that promotes the formation of increasingly elongated cells and filaments by interfering with the formation of the septal ring and stopping cell division (Eberhardt et al, 2003). Cephalexin is not otherwise known to alter growth rate, physiology, or flagellar motility (Rolinson, 1980; Ishihara et al, 1983; Maki et al, 2000). Once cephalexin was added, chemotactic performance was evaluated every hour, as cells progressively elongated, up to five hours after the addition of cephalexin.

Before performing any chemotactic assay, cultures were washed into random motility buffer (RMB) (Turner et al, 2000) by filtering and backwashing with RMB through a 0.2µm sterile membrane three times (Bell et al, 2005). This procedure resulted in highly motile suspensions of bacteria with limited loss of cells (usually less than half) and was much quicker than the classical centrifugation technique.

Microfluidic device

To evaluate the chemotactic ability of *E. coli*, we used an agarose-based microfluidic device with three channels (Fig. 1A, (Diao et al, 2006; Cheng et al, 2007; Ahmed et al, 2010). This design allows the generation of quiescent, steady linear chemical gradients. We used a design with three 600µm wide and 100 µm deep channels running parallel and separated by 200 µm wide walls and embedded in 3% agarose (corresponding to 'design 2' in Ahmed et al, 2010). Details on the fabrication and calibration of the devices are given in supplementary.

Chemotactic assays

In all experiments we kept the concentration of aspartate in the source channel at 100 µM, while changing the concentration at the sink channel to achieve different gradients. We performed experiments with three different sink concentrations (0, 25 and 50 µM) which, after accounting for the differences from theory quantified in the device calibration, resulted in cross-channel average relative concentration gradients of 1.20 mm^{-1}, 0.72 mm^{-1} and 0.40 mm^{-1} respectively. Relative gradients are defined as $\frac{dC}{dx}/\bar{C}$, where C is the concentration of α-methyl-aspartate, x is the distance along the gradient and $\bar{C}$ is the average concentration over the whole width of the channel (see a list of all symbols used throughout the text in table 1). These linear gradients were similar to those considered in previous experimental and theoretical studies of bacterial chemotaxis (e.g., Ahmed & Stocker, 2008; Kalinin et al, 2009).

We imaged cells in a phase contrast inverted microscope (Zeiss AxioVert A1) equipped with a temperature-controlled stage (PE100-ZAL System, Linkam Scientific Instruments Ltd., Tadworth,

UK) and using a 10X objective (0.55 NA), which gave a depth of field of 12.4 µm. Videos were recorded using a sCMOS camera (Hamamatsu ORCAFlash2.8, Hamamatsu City, Japan). The resulting lateral resolution was of 2.75 µm pixel^{-1}, and the field of view was 524 µm by 598 µm, allowing the visualization of almost the entire width of the channel at once. Videos were taken at 30 fps which is fast enough to efficiently track *E. coli* (Guadayol et al, 2017).

In each experiment, several one-minute-long videos were taken at regular intervals starting 10 minutes after bacteria were seeded in the centre channel, giving ample time for the chemical linear gradient to re-establish (Ahmed et al, 2010), and ending 60 minutes after seeding. Motile bacteria were tracked using in-house MATLAB® code described elsewhere (Guadayol et al, 2017) and published under an open-source license (Guadayol, 2016). The code characterizes the shapes and positions of individual cells and registers frequency, duration, speed and direction of runs, as well as frequency, duration and angle of reorientations.

A few minutes after injecting the bacterial culture into the central channel, cells visibly aggregated towards the outer channel with the highest chemoattractant concentration, following an exponential distribution. The inverse of the exponential decay constant, the chemotactic precision length scale (L), was used to parameterize chemotactic performance (Kalinin et al, 2009; Son et al, 2016). Precision length scales were estimated for each cell-length class and chemical gradient by fitting an exponential function to the distribution of bacteria across the centre channel from all recordings that passed the quality control (see below), using the Least Absolute Residual (LAR) robust curve fitting algorithm. Data points less than 50 µm from the walls were discarded because light diffracted by the agarose walls interfered with the particle detection algorithm.

To calculate L we only used time points that fulfilled the following quality control criteria, which we deemed conservative: 1) the residual flow inside the centre channel, resulting from imperfect sealing of the agarose with the PDMS, was below 2 µm s^{-1} (i.e., ~10% of the average speed for *E. coli*); 2) the average number of cells per frame detected was higher than 500; 3) the distribution of cells was monotonically decreasing away from the nutrient source, and 4) the coefficient of

determination R^2 of the fitted exponential model was higher than 0.1.

IBM model

We developed an individual-based model (IBM) to gain a mechanistic insight into how chemotactic responses depend on the cell length. The IBM was written in MATLAB® code and published under GNU license (Guadayol, 2023). The IBM simulates cells behaving independently (i.e., without interacting or communicating with other cells) in a 2D domain bound by parallel reflecting walls 600 µm apart, which is the width of the channel in the experimental microfluidic device. The chemotactic behaviour of the cells in the IBM was simulated with a coarse-grained chemotactic pathway model described extensively elsewhere (Tu et al, 2008; Kalinin et al, 2009; Tu et al, 2010). See *Supplementary methods* for details on our implementation. Both the number of cells (10^5) and the time step (0.1 s) were selected to ensure errors below 10% (see *Convergence tests* in *Supplementary methods).* Each simulation was randomly populated with cells of a given cell length. The number of cells remained constant throughout the simulation. Their swimming speed (v), tumble bias (*TB*, the proportion of time spent tumbling) and directional persistence (α_p, defined here as the average of the cosine of the reorientation angles) were drawn from published empirical functional relationships of these parameters versus cell length for *E. coli* swimming in homogeneous conditions (Guadayol et al, 2017), Figure S1). All parameters used in the IBM are listed in table 1.

During a run, each cell was assumed to move at a constant run speed, while the swimming direction was affected by rotational Brownian motion. To account for this effect, after each time step, the run direction was changed by adding a normally distributed stochastic component with standard deviation $\sigma = \sqrt{2D_r\Delta t}$, where D_r is the size- and shape-dependent rotational diffusivity perpendicular to the long axis and Δt is the time step of the simulation. Rotational diffusivity can be calculated as $D_r = \frac{kT}{f_r}$, where k is the Boltzmann constant, T is the absolute temperature and f_r is the rotational friction coefficient about the short axes. Following Dusenbery (Dusenbery, 1998), we

modelled bacteria as rigid prolate ellipsoids of revolution, and used well-known theoretical solutions for the friction coefficients (Perrin, 1934).

The duration of both runs and tumbles was modulated stochastically from Poisson processes whose frequencies are the inverse of the expected durations and which generate the exponential distributions observed experimentally (Berg & Brown, 1972). The expected duration of a tumble (τ_t) changed only with cell length, while the expected duration of a run (τ_r) depended also on environmental chemoattractant concentrations (see following subsections).

At the start of a simulation, cells were distributed uniformly and aligned randomly within a 600 by 600 µm square domain. A reflecting boundary condition was imposed at the two edges of the domain perpendicular to the nutrient gradient, analogous to the walls of the centre channel in the chemotactic device; our results were insensitive to this choice (see *Boundary behaviour* in supplementary). Cells bumping into one of the two edges parallel to the gradient were translated to the other boundary without a change in course or speed (i.e., a periodic boundary condition).

Phycosphere model

The phycosphere was simulated with the same IBM model on an annular 2D domain, in which the inner circle approximated the wall of a spherical phytoplankton cell of radius 25 µm. Bacteria encountering a boundary bounced away conserving the same angle of incidence and speed.

The chemoattractant concentration gradient around a spherical phytoplankton cell at steady state, assuming background concentrations to be 0, follows $C(r) = C_0 r_0\, r^{-1}$ (e.g., Jackson, 1987), where r is the radial distance from the centre of phytoplankton cell, r_0 is the radius of the cell, and C_0 is the concentration of the chemoattractant at the cell wall. C_0 was set to be constant with an arbitrary value of 10 µM, corresponding to a situation where the cell is releasing the chemoattractant at a constant rate. In this scenario, at steady state the shape of the chemical gradient is independent of molecular diffusivity.

These simulations were 10 minutes long because aggregations of bacteria around nutrient hotspots

commonly form and dissipate over similar periods of time (Blackburn et al, 1998; Smriga et al, 2016).

Results

Experimental results

We detected chemotactic responses in populations of *E. coli* of all cell lengths. These responses were caused by a directional bias in run times rather than in swimming speed (Figure 1C, D) as is commonly observed in *E. coli.* After a few minutes, cells distributed along the chemical gradient following an exponential relationship in all experiments (Figure 1B) of the form $B(x) = B(0)e^{-\frac{x}{L}}$, where $B(x)$ is the cell density at distance x from the wall closest to the most concentrated outer channel, and L is the chemotactic precision length scale that parametrizes how tightly cells aggregate near the source of chemoattractants (Son et al, 2016). The observed exponential distribution is the steady-state solution of the Keller-Segel's bacterial transport model for a linear chemical concentration profile (Kalinin et al, 2009; Son et al, 2016). In this solution, at steady state $L = \mu/v_c$, where μ is the random motility coefficient that parametrizes the diffusivity of bacteria in the absence of chemical gradients, and v_c is the chemotactic drift velocity, i.e., the average speed at which bacteria swim towards the source. Thus, L can be interpreted as the ratio of bacterial diffusivity to chemotactic ability. The shorter L is, the better bacteria are at exploiting a nutrient source.

As previously observed (Kalinin et al, 2009), L decreased with increasing gradient steepness (Figure 2). Regardless of the steepness, the functional response of L to cell length was U-shaped, with minimum L occurring for cells 2.5 to 5 µm long. This supports our hypothesis that some trade-off for optimal chemotaxis is operating in *E. coli*. However, our experimental system alone does not allow identifying which mechanisms are driving the observed pattern for two reasons. First, L is an emerging population parameter that ultimately depends on at least four shape-dependent individual-based motility parameters. These parameters are rotational friction coefficient f_r, swimming speed v,

tumble bias *TB* (that is the proportion of time spent tumbling) and directional persistence α_p (defined here as the average of the cosine of the reorientation angles). All these parameters have non-linear functional relationships with cell length (Figure S1, (Guadayol et al, 2017). Thus, the observed pattern has multiple possible non-mutually exclusive explanations. For example, high *L* could be equally explained by conditions that increase μ, such as high v or α_p, or by conditions that decrease v_c, such as low f_r. A summary of these possible explanations based on current theories is given in the supplementary section *Theoretical background* and in table S1.

The second reason is that we manipulated cells into adopting potentially unnatural shapes, which could induce experimental artefacts. For example, flagella could become increasingly desynchronized as cells elongate, because of the longer distance that chemical signals need to diffuse and because of the difficulty of forming a single bundle when flagella are far apart (Lee et al, 2021). This might lead to changes in *TB* that may partly explain the increase in *L* for the longest cells. However, such experimental artefacts do not necessarily reflect the biophysical constraints on chemotaxis over evolutionary time and make it difficult to generalize results.

Thus, in order to tease apart which parameters are driving the observed pattern, we developed an individual-based model (IBM) that simulates a population of chemotactic bacteria of a given cell length swimming along a linear gradient of aspartate. The model reproduces the main trends observed and shows a good fit with the experimental data for the three chemoattractant gradients explored (Figure 2).

IBM dynamics

In all IBM simulations, *L* monotonically decreased over time, approaching a horizontal asymptote. We defined an operational steady state as the time at which the relative rate of change in *L* was lower than 10% per hour. Allowing simulations to proceed until steady state revealed a trend different to what was observed experimentally: *L* decreased almost monotonically with cell length (grey circles in Figure 3A) instead of showing a local minimum at intermediate cell lengths (Figure

2). The time t_{ss} it took for the simulations to reach steady state, on the other hand, did show a minimum at intermediate lengths.

This suggests that the increase in L for longer cells observed in the experiments reflects the transient nature of the measurements. For practical reasons experiments were run for 60 minutes, which according to the simulations, is insufficient time for the system to reach steady state when cells are longer than 10 µm. Furthermore, L is estimated from bacterial positions throughout the experimental time. A more ecologically relevant parameter to gauge the chemotactic performance of bacteria is likely the population-averaged time-integrated exposure to nutrients N, which again shows a relative advantage of cells of intermediate length even at short time scales (Figure 3C). The advantage of cells of intermediate length over the longest cells, however, diminishes as simulation time increases (Figure S5).

Sensitivity analysis

To understand the role of each motility parameter in the emerging pattern, we performed a sensitivity analysis of the model (Figure 3) using a one-at-a-time (OAT) approach: we ran a series of simulations to steady state in which we changed each one of the relevant shape-dependent parameters (f_r, v, TB, α_p) whilst keeping the other parameters constant at the empirical average values for a wild-type cell 1.7 µm long and 0.75 µm wide at a temperature of 30°C swimming in a homogeneous environment (f_r=0.4·10^{-20} kg m^{2} s^{-2}, v=18 µm s^{-1}, TB=0, α_p=0, Figure S1, (Guadayol et al, 2017)). Note that, since tumble time τ_t is insensitive to changes in chemoattractant in the chemotactic pathway model, responses to TB mostly reflect responses to run time τ_r.

This analysis showed that, at steady state, changes in v, TB and, most importantly, f_r drove decreases in L as cells elongated (Figure 3A). On the other hand, α_p drove increases in L that may moderate the decay in L as cells elongate. The operating trade-offs are more clearly revealed in the steady state time t_{ss} and N (Figure 3B,C): slow performances of short cells are explained by f_r, whereas those of long cells are driven by v and TB. Steady state time remained insensitive to changes in α_p.

Chemotaxis in the phycosphere

One of the most important hotspots of microbial activity in aquatic systems is the phycosphere, the volume influenced by the metabolic activity of a phytoplankton cell (Seymour et al, 2017; Raina et al, 2022). We further used our model to explore which shape may be optimal for chemotactic bacteria seeking phycospheres in the diluted, dynamic and patchy planktonic microenvironment.

We considered the diffusion of a chemoattractant from a 50 µm diameter phytoplankton cell with a constant rate of release and assumed steady state following previous models (Jackson, 1987). In this scenario, concentration does not decrease linearly as in our chemotactic device but as a function of $1/r$, where r is the radial distance to the centre of the phytoplankton cell. We then ran IBM simulations within a 2D plane to model the clustering of bacteria around phytoplankton. The results show bacterial distributions consistently peaking some micrometres away from the phytoplankton cell surface (Figure 4B). This is a behaviour commonly observed in IBMs of chemotaxis and is called the "volcano effect" (e.g., (Bray et al, 2007; Simons & Milewski, 2011). It results from bacteria swimming past the point of maximum concentration of attractant because it takes some time for the cell to detect a decrease in chemoattractant concentration and initiate a tumble. This reaction time is often parameterized by the latency time, which is a measure of the time needed for signals generated by external stimuli to be processed through the complete signal transduction pathway. A sensitivity analysis indicated that while the magnitude of this local peak was sensitive to changes in all motility parameters, its location was most sensitive to swimming speed (Figure S6) because, given chemotactic response time, faster swimming translates into longer reaction distances. Thus, for example, in our modelling framework the distribution of a population of bacteria swimming at 20 µm s^{-1} peaked 40 µm away from the phytoplankton cell wall, whereas that of a population of bacteria swimming at 100 µm s^{-1} peaked 200 µm away.

Again, the time-integrated exposure to nutrients N is a better measure of the ecological relevance of these results. As in the linear gradient case, N increases rapidly with cell elongation up to a length of around 3.3 µm and then decreases more gradually (Figure 4A). To understand this trend, we

explored the 2-D spaces defined by f_r on one axis and v, TB, and α_p on another (Figure 4C-E). This exercise shows that as cells elongate, N is maximized by low TB (i.e., long runs), an α_p close to -1 (characteristic of a run-and-reverse pattern), and a speed v of around 20 µm s^{-1}. Slow swimming leads to slow aggregation around the phytoplankter, but swimming too fast amplifies the volcano effect (Figure S6).

Discussion

Physical constraints and biological trade-offs

The time-integrated exposure to chemoeffectors N, which we consider a measure of fitness of a chemotactic strategy, depends on two factors: the precision and the speed of chemotaxis. All shape-dependent motility parameters affect these two factors in different ways (Figure 3). Chemotactic precision, which we parameterize with the chemotactic precision length-scale L, improves sharply with increasing f_r, and to a lesser extent, with decreasing v and increasing TB. The result is that, at steady state, precision improves as cells elongate. On the other hand, the speed of the chemotactic process, which is inversely related to the time t_{ss} to reach steady state, is positively related to v and f_r and negatively related to TB. The result is that chemotaxis is fastest for *E. coli* cells of 3 to 7 µm in length. Thus, the U-shaped response of L to elongation that we observed empirically likely resulted from shape-dependent motility parameters acting oppositely on the precision versus speed of the chemotactic process, and therefore reflect a well-known trade-off between exploitation and exploration (Clark et al, 2005; Altindal et al, 2011).

The general trends observed in L at steady state in response to changes in f_r, v, and α_p conform to predictions from theoretical models. For example, the response of L to elongation-driven changes in f_r (Figure 3A) is consistent with the monotonic improvement in gradient detection predicted by Dusenbery based purely on length dependant changes in translational and rotational drag in ellipsoids of revolution (Dusenbery, 1998). The decrease in L in response to decreases in v as cells elongate is consistent with the Keller-Segel model, which predicts a positive, linear relationship

between these parameters (Rivero et al, 1989). Finally, the increase in L with increasing α_p as cells elongate is consistent with predictions from Lovely and Dahlquist (Lovely & Dahlquist, 1975), who established a positive relation between α_p and the random motility parameter μ (and hence, also L).

However, the apparently small effect α_p has on L, and particularly on t_{ss} (Figure 3B), is somewhat surprising. Analytical models (Locsei, 2007) predict that maximum chemotactic velocity v_c occurs as α_p approaches 1 (that is, as tumble angles approach 0 degrees), although strictly speaking v_c collapses when $\alpha_p = 1$ because the cell is effectively no longer tumbling. Even though we did not compute v_c, its dependence on α_p should still be reflected both in L (as $L=\mu/v_c$) and in t_{ss}. The small role α_p seems to be playing in the observed trends would suggest that its effect on bacterial diffusivity may be overpowering its effect on chemotactic velocity.

Alternatively, the marginal significance of α_p in our results may also be reflecting its poor performance as a descriptor of reorientation behaviour, at least in peritrichous bacteria such as *E. coli*. Motility patterns are defined by the mode of reorientation between runs. The changes in motility pattern imposed by elongation in *E. coli* are poorly characterized by α_p because it does not discriminate between 180º reorientations and true reversals (where a leading pole in the previous run becomes the trailing pole, as the bundle is reformed in the opposite pole). Thus, for example. α_p=0 could equally result from a truly uniform distribution of tumble angles and from a pattern of angles in which half are 0º and half are 180º. In any case, the relationship between α_p and L needs to be further explored.

Ecological and evolutionary implications

The optimal values for chemotaxis in our simulations may not be directly ecologically representative because the IBM is based on *E. coli*'s chemosensory circuit for aspartate and uses species-specific motility patterns and physiological responses to elongation. We therefore expect our results to be somewhat dependent on species differences in their sensitivity to different chemoattractants and to the magnitude and shape of the chemical gradient, as well as the more

generic aspects of the geometry and boundary conditions of the model domain, and the simulation time. However, we suggest that our results still reflect underlying trade-offs and evolutionary pressures acting on bacterial morphology.

Our results indicate that an optimal value for cell length arises from the well-known trade-off between the need for rapidly tracking nutrient patches (exploration) and the need for remaining close to them (exploitation) (Clark et al, 2005; Altindal et al, 2011). Long cells will eventually maintain a tighter distribution near a nutrient source while short cells will track the gradient faster. Thus, the optimal cell length of bacteria realized in nature will likely depend on the particulars of their environment (Stocker & Seymour, 2012). In environments where gradients are long and stable over time (relative to microbial scales), such as at the sediment-water interface, we may expect selective pressure for remaining close to the nutrient source and therefore for increasing directional control by increasing f_r and α_p. This is consistent with observations of extremely long and large bacteria near and within sediments (Fenchel, 1994; Guerrero et al, 1999; Jørgensen, 2006). In the planktonic environment, with its patchy, dynamic and ephemeral nutrient landscape, speed is likely more important (Xie & Wu, 2014). This may partly explain why the median aspect ratio of planktonic bacteria is relatively small (around three: (Dusenbery, 1998)), and why flagellated bacteria in oligotrophic environments tend to swim faster (Mitchell et al, 1995). This argument, of course, does not reflect the fact that tasks and costs other than chemotaxis may be important for bacterial fitness (Young, 2006; Schuech et al, 2019), nor their interaction with flow (Luchsinger et al, 1999; Taylor & Stocker, 2012).

This need for speed in the planktonic environment may be moderated, as our simulations show, by the occurrence of a volcano effect that penalizes very fast swimmers (Figures 4, S6). The volcano effect results from cells overshooting the phycosphere as it takes some time (the “latency time”) for the bacterial chemotactic pathway to perceive a decrease in chemoattractant concentration and induce reorientation (Bray et al, 2007; Simons & Milewski, 2011). Thus, the importance of the volcano effect depends on three factors: the shape of the chemoattractant gradient, the latency time

and the swimming speed. The slower the cells are at reacting to a change in concentration and the faster they swim, the further from the maximum concentration will their population distribution peak. In our simulations this translates into optimal nutrient exposures at swimming speeds remarkably close to the average value for wild-type *E. coli* (Figure 4C). In general, the latency time will add a constraint on the maximum swimming speed that is ecologically viable in a given planktonic system.

If the volcano effect proves to be an ecologically relevant mechanism, there are several factors that could be reducing its impact in marine bacteria. First, their latency times are thought to be much faster (Stocker, 2011) than those of *E. coli* (~0.2 s Block et al, 1982)). Second, speed-dependent responses such as chemokinesis or changes in motility pattern (Son et al, 2016), which we have not considered here, may help bacteria remain longer around nutrient patches even when their swimming speeds are high. Third, the adoption of swimming patterns with a reversal phase and long runs, which are prevalent among marine bacteria (Johansen et al, 2002) can also maximize nutrient exposure around a phycosphere (Figure 4). And finally, the existence of a viscous layer of exopolymers around a phytoplankton cell may minimize the volcano effect (Guadayol et al, 2021).

Otherwise, our simulations of the phycosphere depict an optimal strategy that is largely consistent with observations of marine bacteria. The simulations predict that elongated cells with a run-and-reverse pattern (i.e., $\alpha_p \rightarrow -1$) and long runs (i.e., $TB \rightarrow 0$) will be most efficient in harvesting nutrients at timescales of tens of minutes (Figure 4). Among marine bacterial populations, the median cell aspect ratio is close to 3 (Dusenbery, 1998), the prevalent motility pattern is run-and-reverse (Johansen et al, 2002) or has some sort of reversal phase (Xie et al, 2011), and the most common type of flagellation is a single polar flagellum (Grognot & Taute, 2021), which favours long runs at the cost of increasing chemotactic response times (Sneddon et al, 2012).

We have focused on individual motility parameters (rotational friction, run speed, tumble and run times, directional persistence) that are dependent on the shapes of the organisms in our experimental system, and that therefore may be expected to change in natural populations

displaying morphological variability. However, cell shape is not the only factor sensitive to selective pressures that can influence these motility parameters. For example, high f_r can also be achieved by means of long flagella, which can act as stabilizers of the running trajectory (Mitchell, 2002; Schuech et al, 2019). Such stabilization would allow cells to be smaller while remaining chemotactically efficient. Similarly, changes in v or α_p can be achieved by means other than elongation, for example by alterations in the number or positions of flagella (Grognot & Taute, 2021). Nevertheless, given the morphological diversity often seen in natural populations, and the ease with which some cell populations appear to change shape, and in particular aspect ratio, varying length may well be a response to an ever-changing nutrient landscape.

Acknowledgements:

This study was funded by Leverhulme Trust project RLA RL-2012-022, “Form and function in a microbial world”, granted to S.H., and by a Gordon and Betty Moore Foundation Marine Microbiology Initiative award, grant 6852 to S.H. and O.G. O.G. was supported by a María Zambrano grant from the University of the Balearic Islands.

Competing Interests: No competing interests are declared.

Tables

Table 1: Summary of the symbols used for each parameter and their definition.

	Symbol	Parameter	Definition	Units
Population-level parameters	C	Chemoattractant concentration	Environmental concentration of aspartate or α-methyl-aspartate	µM
	L	Chemotactic precision length scale	Inverse of the exponential decay constant of bacteria distribution vs distance to nutrient source	µm
	t_{ss}	Time to steady state	Time it takes for IBM simulation to reach steady state, which is defined as the moment when the relative rate of change in L is lower than 10% per hour	min
	B	Normalized cell density	Normalized density of bacteria per distance to source boundary. In the microfluidic device and IBM of it is normalized to number of bacteria in simulation, phycosphere IBM is normalized to initial cell density	-
	N	Normalized nutrient exposure	Time-integrated exposure to chemoattractant for the entire population in IBM simulations, normalized by integrated exposures for non-chemotactic populations distributed uniformly along the gradient	
	μ	Bacterial random motility	Coefficient of diffusivity of a bacterial population in the absence of chemical gradients	$\mu m^2 s^{-1}$
	v_c	Chemotactic speed	Mean speed at which bacteria move up a chemoattractant gradient	$\mu m\ s^{-1}$
Individual motility parameters	f_t	Translational friction coefficient	Translational friction coefficient along the long semiaxis of a prolate ellipsoid of revolution	$kg\ s^{-1}$
	f_r	Rotational friction coefficient	Rotational friction coefficient about the short semiaxes of a prolate ellipsoid of revolution	$kg\ \mu m^2 s^{-1}$
	D_r	Rotational diffusivity	Rate of rotational diffusion about the short semiaxes of a prolate ellipsoid of revolution: $D_r = \frac{kT}{f_r}$	$rad^2 s^{-1}$
	τ_r	Run time	Average duration of runs	s
	τ_t	Tumble time	Average duration of tumbles	s
	TB	Tumble bias	Proportion of time spent tumbling: $TB = \frac{\tau_t}{\tau_t+\tau_r}$	-
	α_p	Directional persistence parameter	Average of the cosine of the reorientation angles	-
	v	Swimming speed	Average swimming speed during runs	$\mu m\ s^{-1}$

Figure legends

Figure 1: Chemotactic responses in example populations of *E. coli* of different cell lengths in a microfluidic device creating a linear gradient of α-methyl-aspartate. **A)** Schematic of the microfluidic device used for the chemotactic assays. **B)** Epifluorescence microscope image of a gradient of fluorescein in the microfluidic device showing the entire width of the central channel where bacteria are located, and partially the lateral channels were buffers with different amount of chemoattractant are flowing. Vertical dashed red lines mark the limits of the channels. Superimposed in green is the profile of average fluorescein concentration (in arbitrary units of fluorescence intensity). **C**) Bacterial cell densities across the width of the central channel for populations of *E. coli* of the three example cell lengths exposed to a linear gradient of α-methyl-aspartate ($\nabla C/\bar{C} = 1.2\mathrm{mm}^{-1}$). The shortest cells (1,7 ±0.3 µm, in purple) are untreated *E. coli* cells. The other two examples correspond to the average length of populations two hours (5.2±1µm, in red) and three hours (13.2±2.4 µm, in orange) after treatment with cephalexin. Circles are empirical measurements; continuous lines are the nonlinear least squares fits of the exponential function (**Error! Reference source not found.**4). **D**) Inverse cumulative frequency of run times for cells swimming upgradient (continuous lines) and downgradient (dashed lines) with a maximum deviation of 45 degrees from the direction of the gradient. **E)** Polar plot of the average run speeds per mean direction of the runs.

Figure 2: Precision length scales *vs*. cell length of *E. coli* populations exposed to linear gradients of α-methyl-aspartate of different steepness. Colours represent the three gradients used in the experiments, blue being the shallowest gradient ($\nabla C/\bar{C} = -0.4\mathrm{mm}^{-1}$), red the intermediate ($\nabla C/\bar{C} = -0.72\ \mathrm{mm}^{-1}$) and purple the steepest ($\nabla C/\bar{C} = -1.2\ \mathrm{mm}^{-1}$). Data points are experimental results, with error bars showing the standard errors of the exponential fits. Coloured areas show the IBM model outputs between 10 (upper limits) and 60 (lower limits) minutes of simulation time.

Figure 3: Sensitivity analyses at steady state of the IBM. **A)** Precision length scales L at steady state; **B)** time t_{ss} it takes for simulations to reach steady state. **C)** Normalized exposures to α-methyl-aspartate N after 30 minutes of simulation time. Gray circles represent simulations where all parameters changed with cell length according to the empirical relationships for cephalexin-treated *E. coli* shown in figure S1. Coloured lines show the results of the one-at-a-time sensitivity analysis, where one parameter varies with cell length while the rest are fixed to the values corresponding to normal-size wild-type *E. coli*.

Figure 4: Modelled chemotactic performances in a phycosphere. **A**) Normalized integrated nutrient exposure (N) after 30 minutes of simulation time, against cell length for simulated populations of *E. coli* around a spherical phytoplankton cell of radius 25 µm releasing Asp at a constant rate. **B**) bacterial densities normalized by background densities vs distance to phytoplankton cell wall. Colour-coded dashed lines represent populations of increasing cell length. The black line represents simulation for a population of wild-type *E. coli* cells displaying a run-and-reverse motility pattern, common in marine planktonic motile bacteria. Run-and-reverse pattern was modelled enforcing a constant tumble angle of 180 degrees for all reorientations. Inset shows the distribution of the chemoattractant Asp used in the simulations. **C-E)** integrated nutrient exposure N as a function of rotational friction coefficient f_r and swimming speed v (C), tumble bias TB (D) and directional persistence α_p (E). While v, TB, and α_p can all be treated as independent of f_r in our simulations, the red lines show the observed dependences derived from experimental work with *E. coli* (Guadayol et al, 2017). Grey line shows the maximum nutrient exposures per rotational diffusion within each two-parameter space.

References

Ahmed T, Shimizu TS, Stocker R (2010). Bacterial Chemotaxis in Linear and Nonlinear Steady Microfluidic Gradients. Nano Lett 10:3379-3385, doi:10.1021/nl101204e.

Ahmed T, Stocker R (2008). Experimental Verification of the Behavioral Foundation of Bacterial Transport Parameters Using Microfluidics. Biophysical Journal 95:4481-4493, doi:10.1529/biophysj.108.134510.

Altindal T, Xie L, Wu X (2011). Implications of Three-Step Swimming Patterns in Bacterial Chemotaxis. Biophysical Journal 100:32-41, doi:10.1016/j.bpj.2010.11.029.

Bell CH, Arora BS, Camesano TA (2005). Adhesion of Pseudomonas putida KT2442 Is Mediated by Surface Polymers at the Nano- and Microscale. Environmental engineering science 22:629-641, doi:10.1089/ees.2005.22.629.

Berg HC, Brown DA (1972). Chemotaxis in *Escherichia coli* analysed by three-dimensional tracking. Nature 239:500-504, doi:10.1038/239500a0.

Blackburn N, Fenchel T, Mitchell J (1998). Microscale Nutrient Patches in Planktonic Habitats Shown by Chemotactic Bacteria. Science 282:2254-2256, doi:10.1126/science.282.5397.2254.

Block SM, Segall JE, Berg HC (1982). Impulse responses in bacterial chemotaxis. Cell 31:215-226, doi:10.1016/0092-8674(82)90421-4.

Bray D, Levin MD, Lipkow K (2007). The Chemotactic Behavior of Computer-Based Surrogate Bacteria. Current Biology 17:12-19, doi:10.1016/j.cub.2006.11.027.

Cheng S, Heilman S, Wasserman M, Archer S, Shuler ML, Wu M (2007). A hydrogel-based microfluidic device for the studies of directed cell migration. 7, doi:10.1039/b618463d.

Clark DA, Grant LC, Berg HC (2005). The bacterial chemotactic response reflects a compromise between transient and steady-state behavior. PNAS 102:9150-9155, doi:10.1073/pnas.0407659102.

Diao J, Young L, Kim S, Fogarty EA, Heilman SM, Zhou P, *et al.* (2006). A three-channel microfluidic device for generating static linear gradients and its application to the quantitative analysis of bacterial chemotaxis. Lab Chip 6:381-388, doi:10.1039/B511958H.

Dusenbery DB (2009). Living at Micro Scale: The Unexpected Physics of being Small. Harvard University Press.

Dusenbery DB (1998). Fitness landscapes for effects of shape on chemotaxis and other behaviors of bacteria. 180:5978-5983.

Eberhardt C, Kuerschner L, Weiss DS (2003). Probing the catalytic activity of a cell division-specific transpeptidase in vivo with β-lactams. J Bacteriol 185:3726-3734.

Erill I, Campoy S, Barbé J (2007). Aeons of distress: an evolutionary perspective on the bacterial SOS response. FEMS Microbiology Reviews 31:637-656, doi:10.1111/j.1574-6976.2007.00082.x.

Fenchel T (1994). Motility and chemosensory behaviour of the sulphur bacterium *Thiovulum majus*. 140:3109-3116, doi:10.1099/13500872-140-11-3109.

Grognot M, Taute KM (2021). More than propellers: how flagella shape bacterial motility behaviors. Current Opinion in Microbiology 61:73-81, doi:10/gjwcbr.

Guadayol Ò (2023). oscar-guadayol/chemotaxisIBM. , doi:10.5281/ZENODO.8360667.

Guadayol Ò, Mendonca T, Segura-Noguera M, Wright AJ, Tassieri M, Humphries S (2021). Microrheology reveals microscale viscosity gradients in planktonic systems. PNAS 118, doi:10/ghsc3s.

Guadayol Ò, Thornton KL, Humphries S (2017). Cell morphology governs directional control in swimming bacteria. Scientific reports 7:s41598-017, doi:10.1038/s41598-017-01565-y.

Guadayol Ò (2016). trackbac: First release.

Guerrero R, Haselton A, Sole M, Wier A, Margulis L (1999). Titanospirillum velox: a huge, speedy, sulfur-storing spirillum from Ebro Delta microbial mats. Proc Natl Acad Sci U S A 96:11584-11588, doi:10.1073/pnas.96.20.11584.

Ishihara A, Segall JE, Block SM, Berg HC (1983). Coordination of flagella on filamentous cells of *Escherichia coli*. J Bacteriol 155:228-237.

Jackson GA (1987). Simulating chemosensory responses of marine microorganisms. Limnol Oceanogr 32:1253-1266, doi:10.4319/lo.1987.32.6.1253.

Johansen JE, Pinhassi J, Blackburn N, Zweifel UL, Hagström A (2002). Variability in motility characteristics among marine bacteria. Aquatic Microbial Ecology 28:229-237, doi:10.3354/ame028229.

Jørgensen BB (2006). Bacteria and Marine Biogeochemistry. In: Marine Geochemistry. Springer Berlin Heidelberg: Berlin, Heidelberg, pp 169-206.

Kalinin YV, Jiang L, Tu Y, Wu M (2009). Logarithmic Sensing in Escherichia coli Bacterial Chemotaxis. 96:2439-2448.

Lee W, Kim Y, Peskin CS, Lim S (2021). A novel computational approach to simulate microswimmers propelled by bacterial flagella. Physics of fluids (1994) 33, doi:10.1063/5.0069343.

Locsei JT (2007). Persistence of direction increases the drift velocity of run and tumble chemotaxis. J Math Biol 55:41-60, doi:10.1007/s00285-007-0080-z.

Lovely PS, Dahlquist FW (1975). Statistical measures of bacterial motility and chemotaxis. Journal of Theoretical Biology 50:477-496, doi:10.1016/0022-5193(75)90094-6.

Luchsinger RH, Bergersen B, Mitchell JG (1999). Bacterial Swimming Strategies and Turbulence. Biophysical Journal 77:2377-2386, doi:10.1016/S0006-3495(99)77075-X.

Maki N, Gestwicki JE, Lake EM, Kiessling LL, Adler J (2000). Motility and chemotaxis of filamentous cells of *Escherichia coli*. J Bacteriol 182:4337-4342, doi:10.1128/JB.182.15.4337-4342.2000.

Mitchell JG, Pearson L, Bonazinga A, Dillon S, Khouri H, Paxinos R (1995). Long lag times and high velocities in the motility of natural assemblages of marine bacteria. Applied and Environmental Microbiology 61:877-882, doi:10.1128/AEM.61.3.877-882.1995.

Mitchell JG, Kogure K (2006). Bacterial motility: links to the environment and a driving force for microbial physics. FEMS microbiology ecology 55:3-16, doi:10.1111/j.1574-6941.2005.00003.x.

Mitchell JG (2002). The energetics and scaling of search strategies in bacteria. Am Nat 160:727-740, doi:10.1007/BF02540225.

Nicolau DV, Armitage JP, Maini PK (2009). Directional persistence and the optimality of run-and-tumble chemotaxis. Computational Biology and Chemistry 33:269-274, doi:10/chfkjq.

Perrin F (1934). Mouvement brownien d'un ellipsoide - I. Dispersion diélectrique pour des molécules ellipsoidales. 5:497-511, doi:10.1051/jphysrad:01934005010049700.

Raina J, Lambert BS, Parks DH, Rinke C, Siboni N, Bramucci A, *et al*. (2022). Chemotaxis shapes the microscale organization of the ocean's microbiome. Nature (London) 605:132-138, doi:10.1038/s41586-022-04614-3.

Rivero MA, Tranquillo RT, Buettner HM, Lauffenburger DA (1989). Transport models for chemotactic cell populations based on individual cell behavior. Chemical Engineering Science 44:2881-2897, doi:10.1016/0009-2509(89)85098-5.

Rolinson GN (1980). Effect of β-lactam antibiotics on bacterial cell growth rate. 120:317-323, doi:10.1099/00221287-120-2-317.

Schuech R, Hoehfurtner T, Smith DJ, Humphries S (2019). Motile curved bacteria are Pareto-optimal. PNAS 116:14440-14447, doi:10.1073/pnas.1818997116.

Segall JE, Ishihara A, Berg HC (1985). Chemotactic signaling in filamentous cells of *Escherichia coli*. J Bacteriol 161:51-59.

Seymour JR, Amin SA, Raina J, Stocker R (2017). Zooming in on the phycosphere: the ecological interface for phytoplankton–bacteria relationships. Nature microbiology 2:17065, doi:10.1038/nmicrobiol.2017.65.

Simons JE, Milewski PA (2011). The volcano effect in bacterial chemotaxis. Mathematical and Computer Modelling 53:1374-1388, doi:10.1016/j.mcm.2010.01.019.

Smriga S, Fernandez VI, Mitchell JG, Stocker R (2016). Chemotaxis toward phytoplankton drives organic matter partitioning among marine bacteria. Proceedings of the National Academy of Sciences - PNAS 113:1576-1581, doi:10.1073/pnas.1512307113.

Sneddon MW, Pontius W, Emonet T (2012). Stochastic coordination of multiple actuators reduces latency and improves chemotactic response in bacteria. 109:805-810, doi:10.1073/pnas.1113706109.

Son K, Menolascina F, Stocker R (2016). Speed-dependent chemotactic precision in marine bacteria. PNAS 113:8624-8629, doi:10.1073/pnas.1602307113.

Stocker R, Seymour JR (2012). Ecology and Physics of Bacterial Chemotaxis in the Ocean. Microbiology and Molecular Biology Reviews 76:792-812, doi:10.1128/MMBR.00029-12.

Stocker R (2011). Reverse and flick: Hybrid locomotion in bacteria. PNAS 108:2635-2636, doi:10.1073/pnas.1019199108.

Taylor JR, Stocker R (2012). Trade-Offs of Chemotactic Foraging in Turbulent Water. Science (80-) 338:675-679.

Tu Y, Shimizu TS, Berg HC (2010). A modular gradient□sensing network for chemotaxis in Escherichia coli revealed by responses to time□varying stimuli. Molecular systems biology 6:382-n/a, doi:10.1038/msb.2010.37.

Tu Y, Shimizu TS, Berg HC (2008). Modeling the chemotactic response of Escherichia coli to time-varying stimuli. PNAS 105:14855-14860, doi:10.1073/pnas.0807569105.

Turner L, Ryu WS, Berg HC (2000). Real-time imaging of fluorescent flagellar filaments. J Bacteriol 182:2793-2801, doi:10.1128/JB.182.10.2793-2801.2000.

Vadia S, Levin PA (2015). Growth rate and cell size: a re-examination of the growth law. Current opinion in microbiology 24:96-103, doi:10.1016/j.mib.2015.01.011.

Willis L, Huang KC (2017). Cell Size: Fat Makes Cells Fat. Current Biology 27:R592-R594, doi:10.1016/j.cub.2017.05.017.

Xie L, Wu X (2014). Bacterial Motility Patterns Reveal Importance of Exploitation over Exploration in Marine Microhabitats. Part I: Theory. Biophysical Journal 107:1712-1720, doi:10.1016/j.bpj.2014.07.058.

Xie L, Altindal T, Chattopadhyay S, Wu X (2011). Bacterial flagellum as a propeller and as a rudder for efficient chemotaxis. PNAS 108:2246-2251, doi:10.1073/pnas.1011953108.

Young KD (2006). The selective value of bacterial shape. Microbiol Mol Biol Rev 70:660-703, doi:10.1128/MMBR.00001-06.

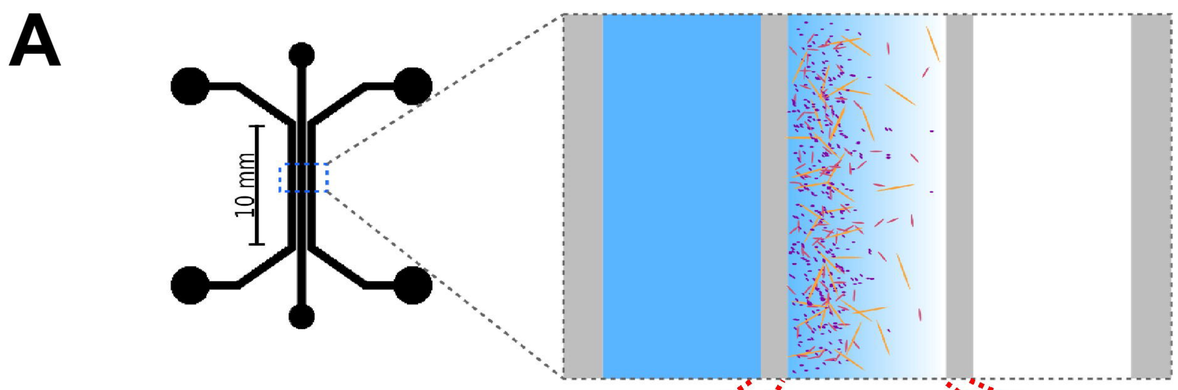
A
10 mm

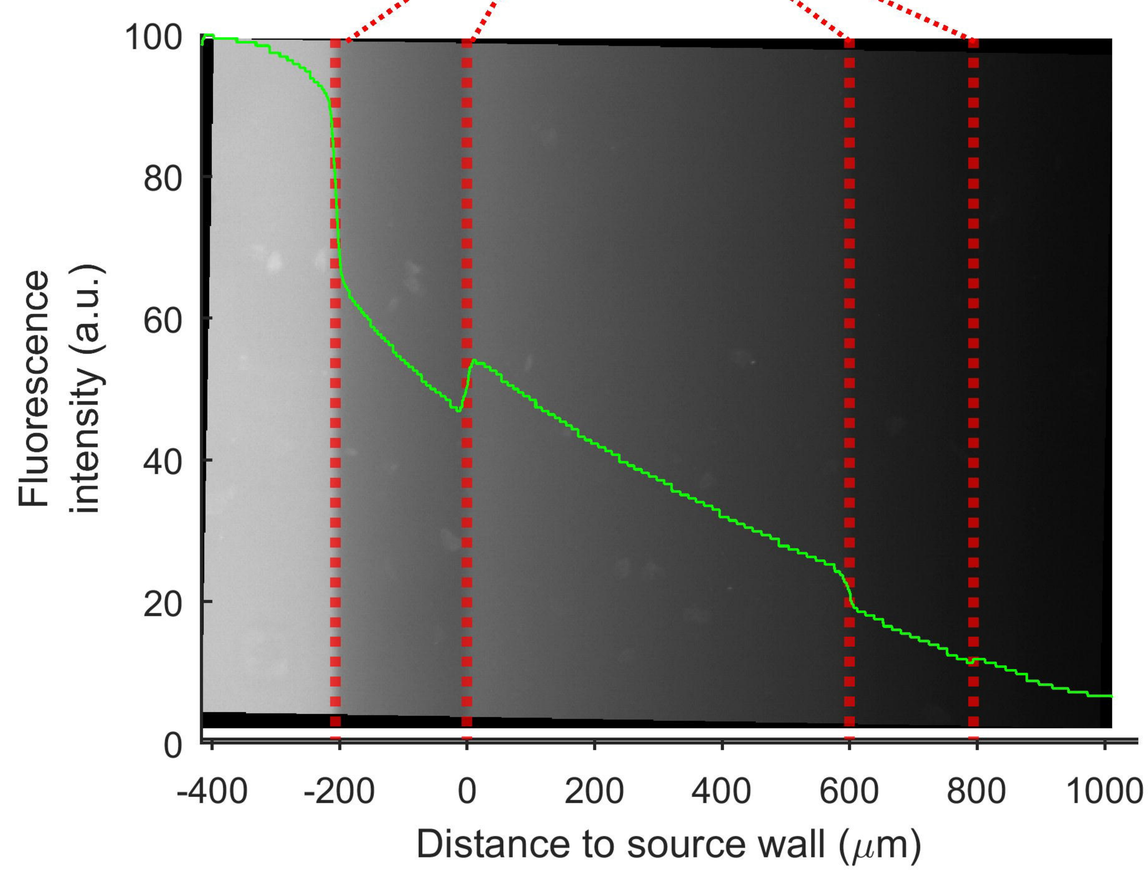
B
Fluorescence intensity (a.u.)
100
80
60
40
20
0
-400
-200
0
200
400
600
800
1000
Distance to source wall (μm)

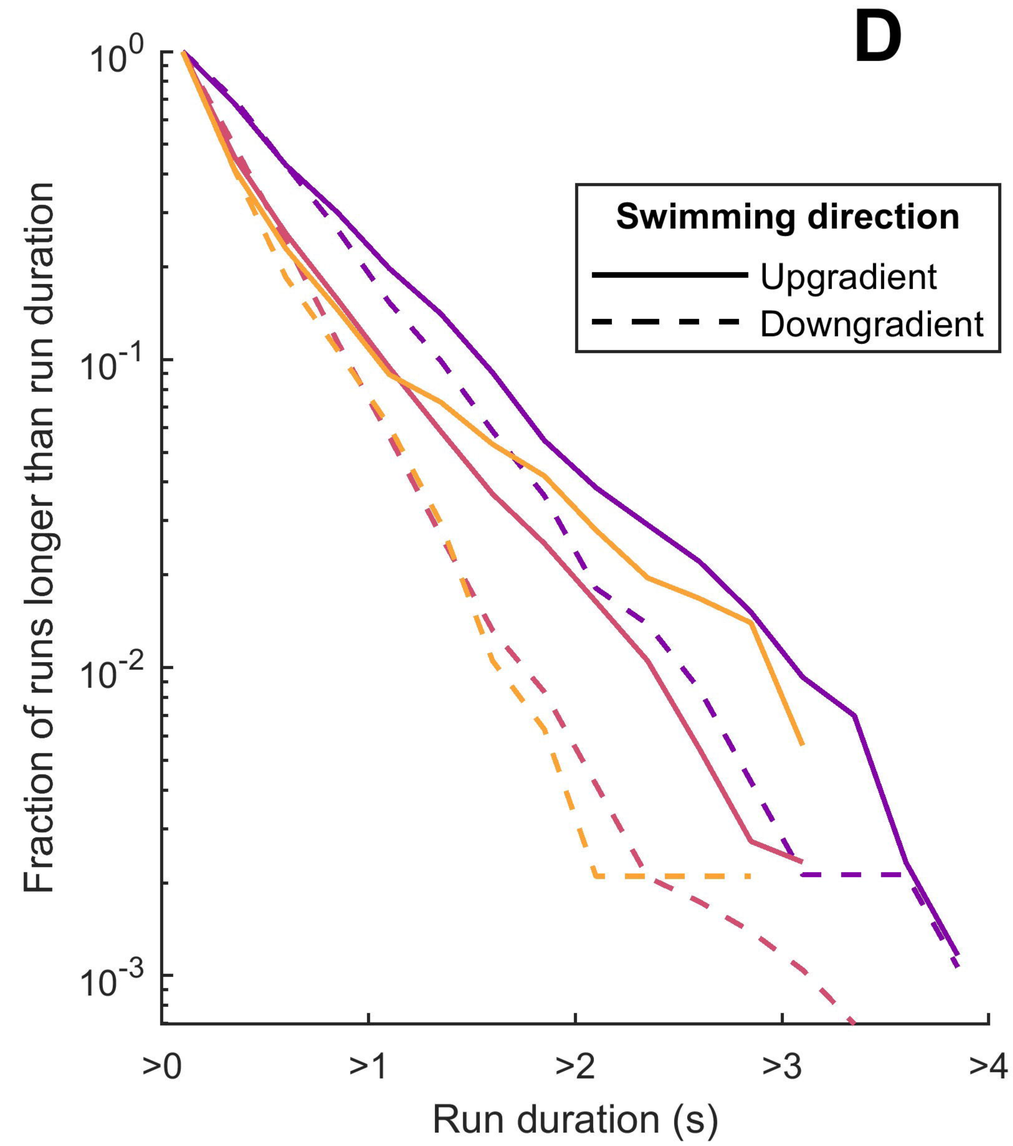
D
Fraction of runs longer than run duration
10^0
10^{-1}
10^{-2}
10^{-3}
>0
>1
>2
>3
>4
Run duration (s)
Swimming direction
Upgradient
Downgradient

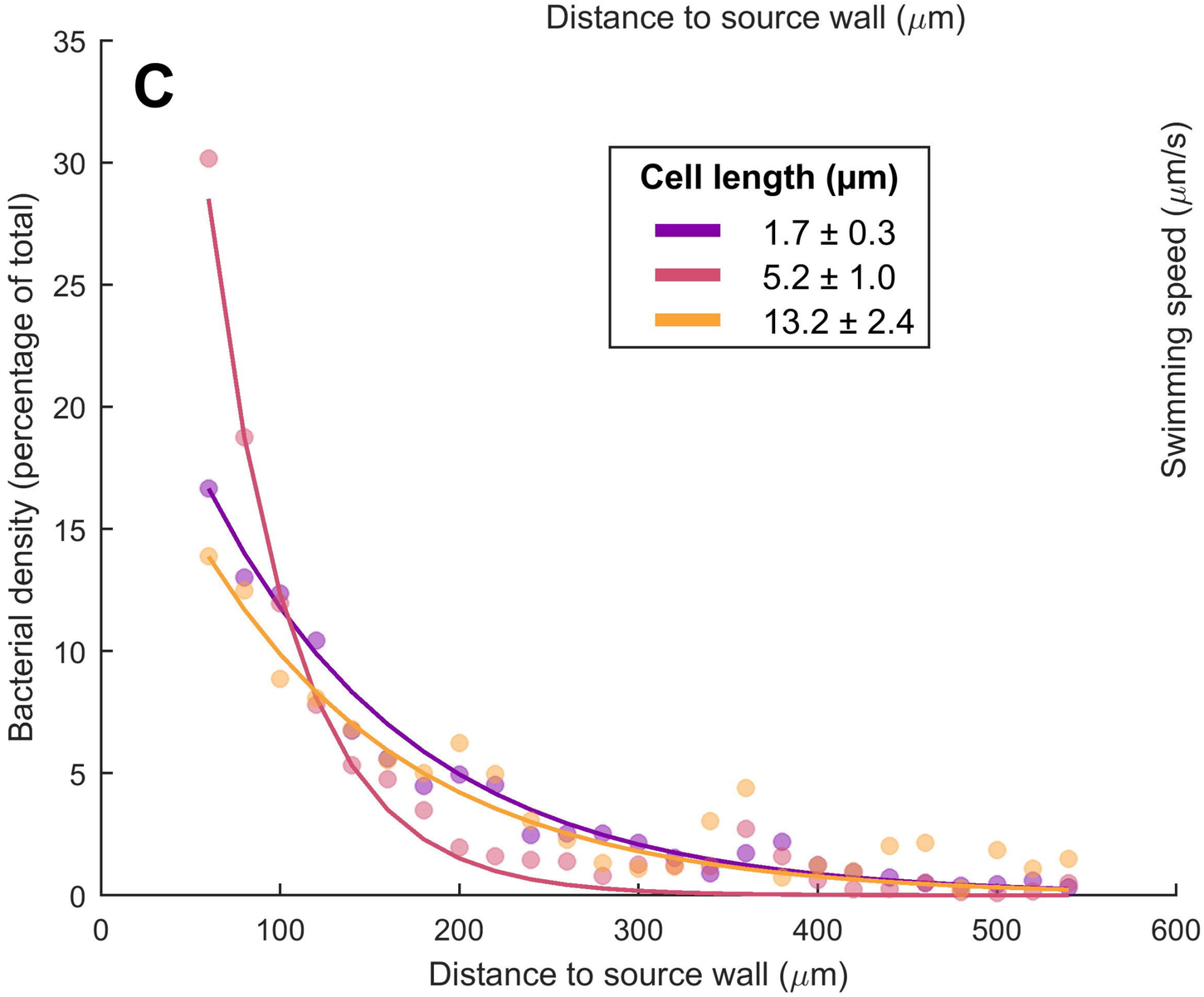
C
Bacterial density (percentage of total)
35
30
25
20
15
10
5
0
0
100
200
300
400
500
600
Distance to source wall (μm)
Cell length (μm)
1.7 ± 0.3
5.2 ± 1.0
13.2 ± 2.4

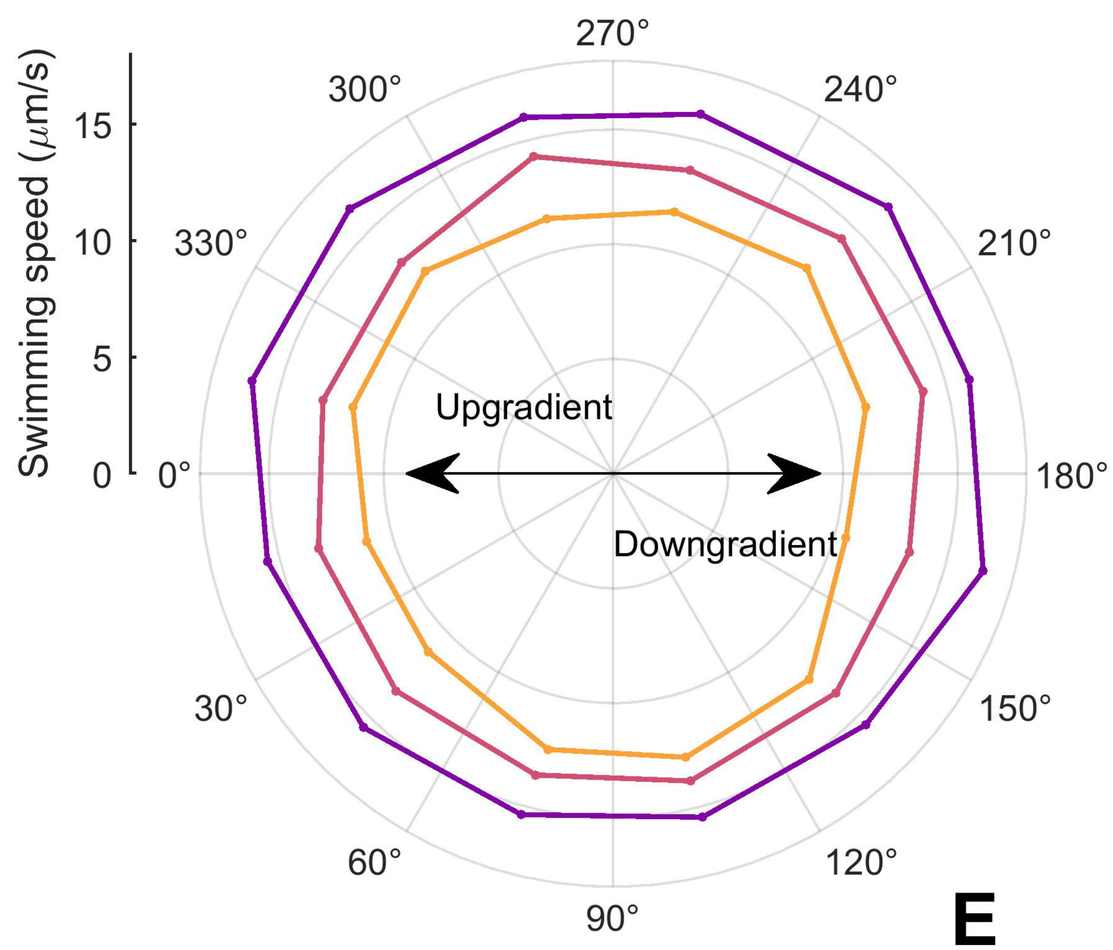
E
Swimming speed (μm/s)
15
10
5
0
270°
240°
210°
180°
150°
120°
90°
60°
30°
0°
330°
300°
Upgradient
Downgradient

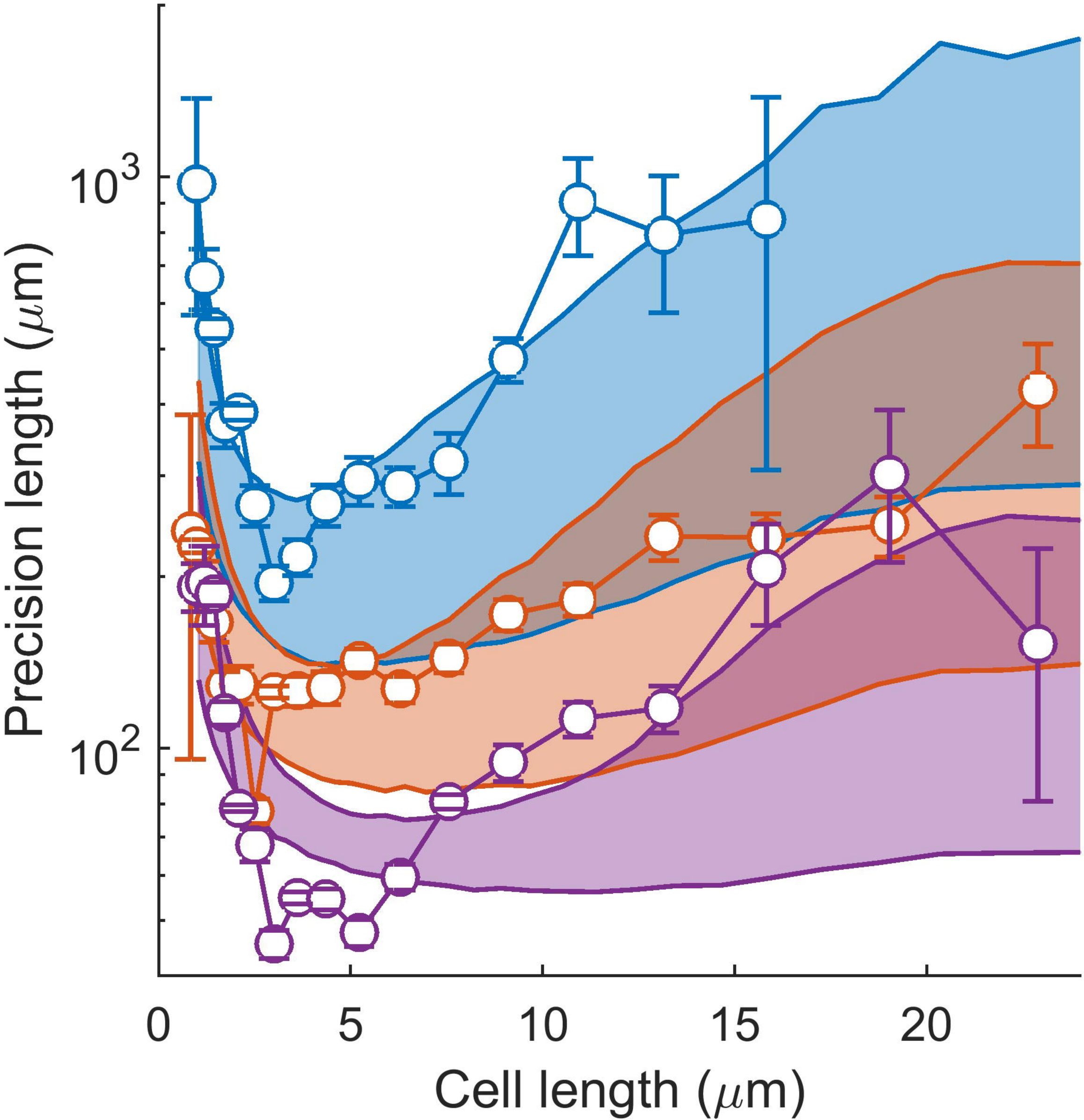
Precision length (μm)
10^3
10^2
0
5
10
15
20
Cell length (μm)

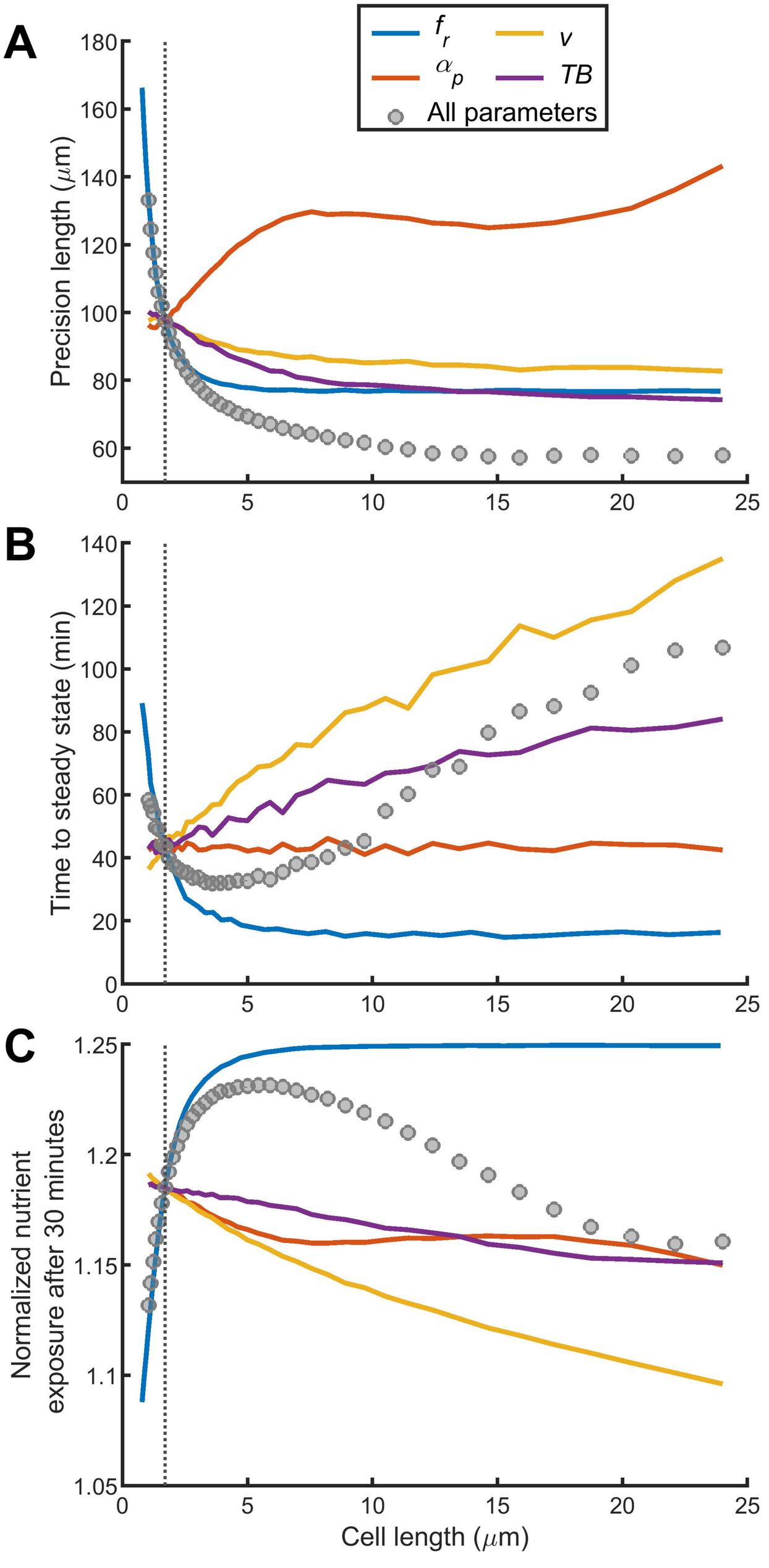
A
B
C
f_r
α_p
v
TB
All parameters
Precision length (μm)
Time to steady state (min)
Normalized nutrient exposure after 30 minutes
Cell length (μm)
180
160
140
120
100
80
60
140
120
100
80
60
40
20
0
1.25
1.2
1.15
1.1
1.05
0
5
10
15
20
25

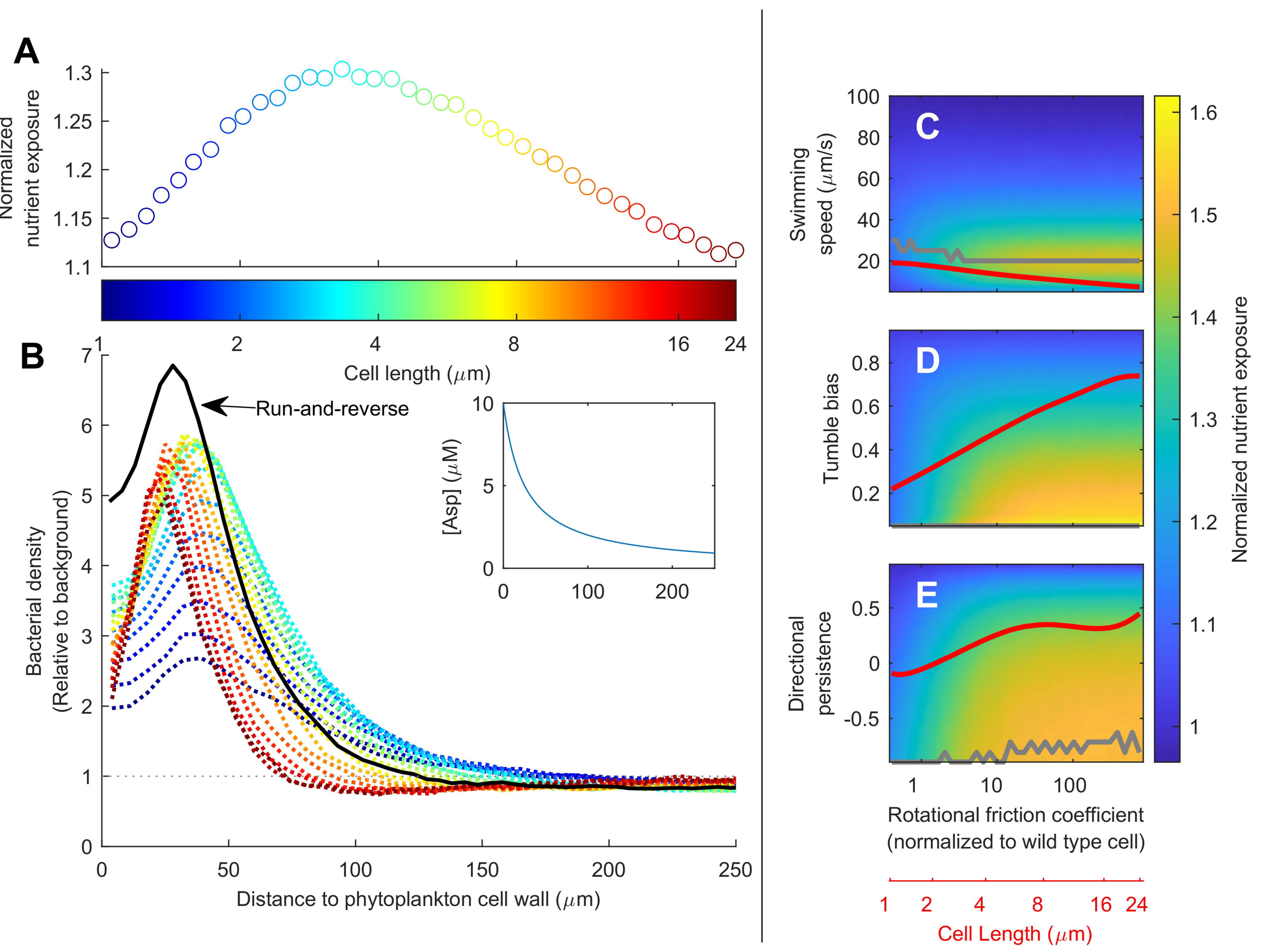
A
Normalized nutrient exposure
1.3
1.25
1.2
1.15
1.1
1
2
4
8
16
24
Cell length (μm)
B
Bacterial density (Relative to background)
Run-and-reverse
[Asp] (μM)
10
5
0
0
100
200
0
50
100
150
200
250
Distance to phytoplankton cell wall (μm)
C
Swimming speed (μm/s)
100
80
60
40
20
D
Tumble bias
0.8
0.6
0.4
0.2
E
Directional persistence
0.5
0
-0.5
1
10
100
Rotational friction coefficient (normalized to wild type cell)
1
2
4
8
16
24
Cell Length (μm)
Normalized nutrient exposure
1.6
1.5
1.4
1.3
1.2
1.1
1